crystallization, composition gradients, hybrid lamination, and functionally graded or layered coatings.

References and Notes

1. D. J. Green, *Introduction to Mechanical Properties of Ceramics* (Cambridge Univ. Press, Cambridge, UK, 1998).
2. B. R. Lawn, *Fracture of Brittle Solids* (Cambridge Univ. Press, Cambridge, UK, ed. 2, 1993).
3. K. Matsuno, K. Shukuri, T. Nakazumi, K. Matsumoto, K. Sono, paper (25-G-87F) presented at the Glass Division of the American Ceramic Society, Fall Meeting, Bedford Springs, PA, 30 September to 2 October 1987.
4. R. Tandon and D. J. Green, *J. Am. Ceram. Soc.* **74** (no. 8), 1981 (1991).
5. _____, *J. Mater. Res.* **7** (no. 3), 765 (1992).
6. _____, in *Crack Stability on Residually-Stressed Surfaces, The Physics of Non-Crystalline Solids*, L. D. Pye, W. C. LaCourse, H. J. Stevens, Eds. (Taylor & Francis, London, 1992), pp. 659–63.
7. R. Tandon, D. J. Green, R. F. Cook, *Acta Metall.* **41** (no. 2), 399 (1993).
8. A. V. Virkar, *J. Am. Ceram. Soc.* **73** (no. 7), 2100 (1990).
9. R. Tandon and D. J. Green, *ibid.* **73** (no. 9), 2628 (1990).
10. E. K Beauchamp and S. J. Glass, personal communication.
11. C.-Y. Hui, S. L. Phoenix, L Kogan, *J. Mech. Phys. Solids* **44** (no. 10), 1715 (1996).

12. We acknowledge the technical assistance of C. Camin and L. Larentis (Università di Trento), the financial support of the Department of Energy under grant 86ER45252 in funding the theoretical calculations, NATO for a collaboration grant (D.J.G. and V.M.S.), and the Deike Foundation (Penn State University).

30 October 1998; accepted 13 January 1999

High-Resolution Water Vapor Mapping from Interferometric Radar Measurements

Ramon F. Hanssen,[1]* Tammy M. Weckwerth,[2] Howard A. Zebker,[3] Roland Klees[1]

Spaceborne radar interferometric delay measurements were used to infer high-resolution maps of integrated atmospheric water vapor, which can be readily related to meteorological phenomena. Maps of the water vapor distribution associated with a precipitating cloud, a partly precipitating cold front, and horizontal convective rolls reveal quantitative measures that are not observed with conventional methods, and suggest that such radar observations can be used for forecasting and to study atmospheric dynamics.

The spatial distribution of water vapor in Earth's atmosphere is important for climate studies (*1*), mesoscale meteorology (*2*, *3*), and numerical forecasting (*2*). Although extensive ground-based and upper-air sounding networks and spaceborne radiometers are routinely used, these measure the water vapor distribution only at coarse scales. These limitations form the main source of error in short-term (0- to 24-hour) precipitation forecasts (*2*). For example, thunderstorm initiation and strength are sensitive to spatial and temporal variations in moisture of the order of 1 g per kilogram of dry air (1.2 hPa) and temperature of 1° to 3°C (*3*, *4*). Such variations are common on a 1-km spatial scale (*5*). Spaceborne synthetic aperture radar (SAR), however, provides horizontal resolution as fine as 10 m over a swath typically 100 km wide (*6*).

The delay variation of SAR signals propagating through the atmosphere can be measured by using the interferometric combination of two observations over most land and rigid ice areas. Over water or other highly changeable surfaces the interferometric method does not work (*7*). SAR interferometry has been used successfully for geophysical applications, such as topographic mapping (*8*, *9*) and deformation measurements (*6*, *10–12*). Atmospherically induced distortion has been observed in these applications (*13–16*) but has typically been treated as noise. Signal delay can be analyzed by eliminating the influence of topography using a reference elevation model (*11*, *14*) and by diminishing the chance of surface deformation by using radar data pairs acquired within a relatively short interval (1 day or less). Then, the observed signal can be interpreted uniquely as the superposition of the atmospheric delay signal during the two acquisitions.

The time, or phase, delay of radar signals in the clear atmosphere consists of ionospheric, hydrostatic, and "wet" components (*17*, *18*). Although the latter is the smallest of these in magnitude (<300 mm) (*19*), it is far more spatially variable than the hydrostatic and ionospheric delays. At spatial scales of less than about 50 km, the interferogram phase will track mainly lateral variation of the wet delay (*20*). Temperature-induced delay variation can be observed, for example, associated with fronts, and is, as such, often easy to identify. Under normal meteorological conditions, however, the magnitude of the temperature effect is small compared with the water vapor signal, because the sensitivity of the refractivity for a change in temperature of 1°C is about one-fourth to one-twentieth the sensitivity to a 1-hPa change in the water vapor pressure. Typically, cloud droplets can produce a maximum delay of several millimeters, whereas the influence of ice crystals can be neglected for the 5-cm radar wavelengths used here (*21*).

Three SAR interferograms obtained over the Netherlands (Fig. 1) show several prominent and representative features. The SAR data were acquired by the ERS-1 and ERS-2 satellites, operating in a 1-day interval mode, ensuring sufficiently coherent images over land areas (*20*). The principal ground resolution of 4 m by 20 m is spatially averaged to 160 m by 160 m, reducing the delay standard error from about 3 mm (*22*) to below 1 mm (*6*).

The signature of a precipitating cumulonimbus cloud is shown in Fig. 2A as a localized delay difference in the SAR line of sight caused by the cloud and the saturated subcloud layer. Using the method described in (*18*, *23*) and a simple cosine mapping function (*21*), we mapped the delay differences to differences in zenith-integrated precipitable water (ΔIPW), the vertically integrated water vapor liquid equivalent. The positive sign of the delay indicates that the feature appeared in the first of the two combined SAR images. This inference was verified by the weather

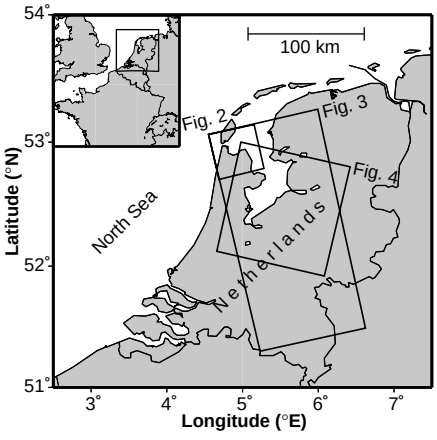

Fig. 1. The location of the discussed radar interferograms. Figure 2 is located at the small square in the upper left corner of the rectangle, Fig. 3 is indicated by the large rectangle, and Fig. 4 by the big square.

[1]Delft Institute for Earth-Oriented Space Research, Delft University of Technology, Thijsseweg 11, 2629 JA Delft, The Netherlands. [2]National Center for Atmospheric Research, Boulder, CO 80307–3000, USA. [3]Departments of Geophysics and Electrical Engineering, Stanford University, Stanford, CA 94305, USA.

*To whom correspondence should be addressed. E-mail: hanssen@geo.tudelft.nl

radar reflectivity signal, expressed as rain rate, on the first day (Fig. 2B). During the second SAR acquisition, no precipitation was observed in the weather radar data. Surface observations and radiosonde data estimated that the cloud base height was 800 m; weather radar data indicated that cloud tops were as high as 4.5 km.

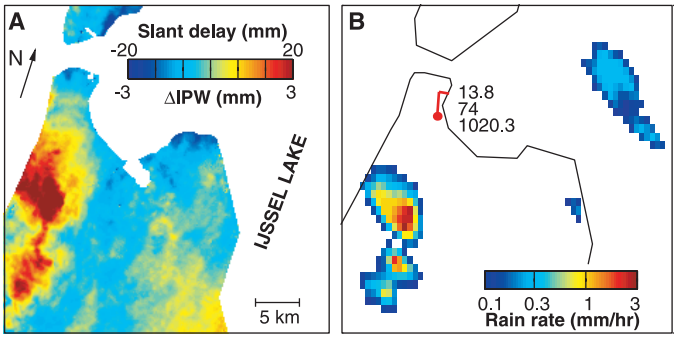

Fig. 2. Images of precipitation. (**A**) The SAR interferogram (29 and 30 August 1995, 21:41 UTC) shows slant delay variation, mapped to zenith-integrated precipitable water differences. The average of the undisturbed area is set to zero, yielding relative precipitable water estimates. (**B**) The weather radar rain rate (29 August 1995, 21:45 UTC). The surface wind velocity was 4.1 m/s, from 350°, indicated by the wind barb. Temperature (in degrees Celsius), the percentage of relative humidity, and pressure (in hectopascals) are plotted beside the station.

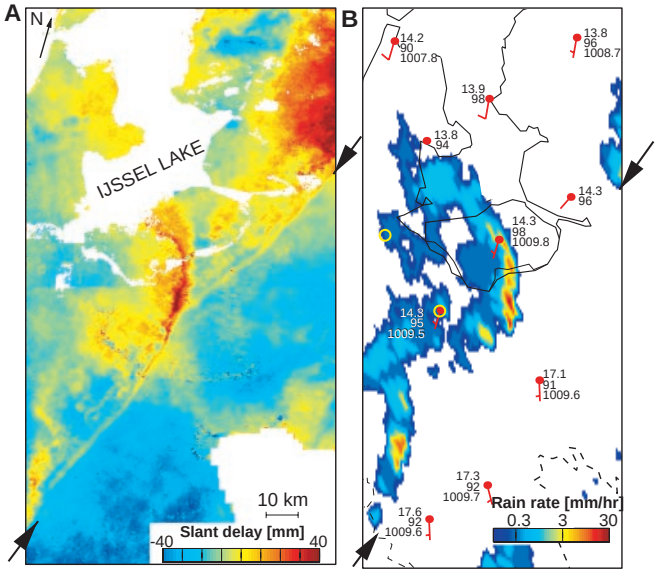

Fig. 3. The effect of a cold front. (**A**) SAR interferogram of 3 and 4 October 1995, 21:41 UTC. The boundary of the cold front is visible as the line between the arrows. Water areas and areas where no elevation data were available are shown in white. (**B**) Weather radar image from 4 October 1995, 21:45 UTC. The positions of the two weather radar stations are indicated by the yellow circles. Superposed are the surface observations (22:00 UTC) as in Fig. 2B. A half wind barb corresponds to 2.5 m/s and a full barb to 5 m/s.

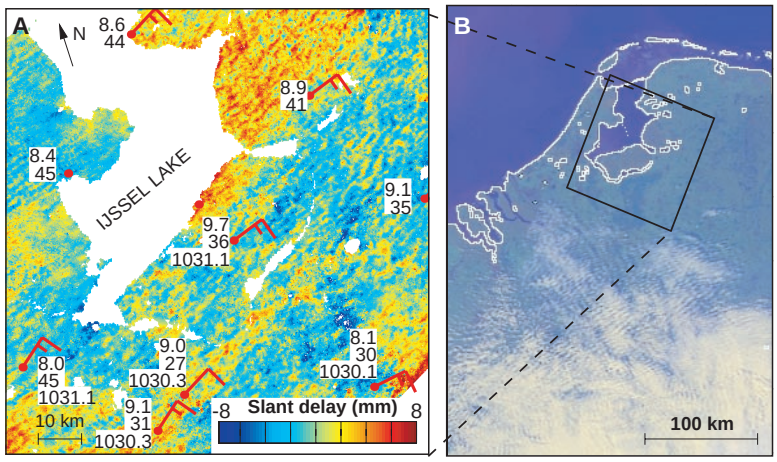

Fig. 4. (**A**) SAR interferogram of 4 and 5 April 1996, 10:35 UTC, showing "water vapor streets," caused by horizontal convective rolls. Surface station observations of 4 April, 11:00 UTC, are superposed as in Fig. 3B. (**B**) Radiometer (NOAA-AVHRR, channels 1, 2, and 4) color composite image acquired at 4 April 1996, 12:01 UTC.

The shape and magnitude of the anomaly in the interferogram correspond closely to the weather radar echo. Phase variations over areas with no precipitation suggest that water vapor gradients are seen in the interferogram that are not observable by the weather radar. The ΔIPW signal over the cloud has a mean value of 1.3 mm, which is reasonably close to the 0.9 mm value inferred from a radiosonde profile, considering it was launched about 90 km away and 4 hours before the SAR overpass. The interferometric technique can measure only relative changes in water vapor; nonetheless, the data reveal that this storm system has about 2.6×10^8 liters more water compared with the surrounding air. For this system to reach equilibrium, this excess water would have to be redistributed over a larger area or precipitate out. Such numerical constraints form important information for forecasting purposes.

A cold front, propagating from the northwest, is shown in Fig. 3A. The interferogram reveals a narrow diagonal band of enhanced water vapor, suggesting the presence of a narrow cold-frontal rain band (*24*). The weather radar data (Fig. 3B), however, show that only parts of the band are precipitating. Surface winds (Fig. 3B) indicate some convergence at the cold front. The frontal circulation may have produced a localized maximum in magnitude or depth of water vapor at the convergence zone, visible as the yellow band in the interferogram. Studies using in situ aircraft and radiosonde observations suggest that regions of enhanced moisture may occur at low-level convergence zones (*25*). The sickle-shaped area visible at the southern end of IJssel Lake likely reflects an evaporatively cooled surface outflow (gust front) generated by the rain showers.

The postfrontal, relatively cold and humid air produces a delay of about 28 mm compared with the prefrontal, relatively warm air. This increase is partly caused by an overall temperature difference of about 3°C associated with the two air masses. The frontal band is 3 to 5 km wide and has an average increase in delay between 11 and 64 mm. With a cold-front depth of 3 km, this delay could be produced either by a 3-hPa increase in water vapor or by an unreasonably large temperature decrease (10°C) at the frontal boundary. Additionally, the contribution of liquid water in a cumulus cloud line would produce a maximum delay difference of less than 2 mm (*26*). Thus water vapor, rather than temperature or liquid water, is likely the primary mechanism causing the increased delay at the frontal boundary.

The areas with delay differences of more than 30 mm correspond to precipitation regions. The sudden increase of water vapor content in the subcloud layer, caused by partial evaporation of the precipitation, accounts for this in-

crease. The liquid cloud and rain particles cannot produce the enhanced delay, because the precipitating clouds would have to be more than 21 km deep to account for the maximum observed delay of 64 mm. The observed features in the interferogram illustrate how localized areas with an increased water vapor content may give an indication for the occurrence and development of precipitation.

The interferogram in Fig. 4 illustrates the frequently occurring phenomenon of horizontal convective rolls, a form of boundary-layer convection in which there are counter-rotating horizontal vortices with axes aligned along the mean boundary-layer wind direction (*27, 28*). Some evidence that the linear features of the interferogram depict rolls rather than atmospheric waves is that the bands are oriented along the wind direction, as shown by the surface station data overlaid on the interferogram (Fig. 4A). Moreover, radiometer satellite imagery (Fig. 4B) to the south of the interferogram location shows some evidence of cloud streets oriented with the interferogram bands. Sufficient moisture in the presence of rolls often produces cloud streets atop roll updraft branches (*29*). Furthermore, a local radiosonde on 4 April 1996 at 12:00 UTC indicated a boundary-layer depth of 800 m. This result, combined with the band spacing of 2 to 3 km, gives an aspect ratio of 2.5 to 2.9, consistent with the presence of rolls (*30*).

Roll updrafts are warmer and moister than roll downdraft branches (*5*). Moisture variability is likely dominant in the observed 6- to 10-mm delay differences, because vapor pressure variations associated with rolls (3 hPa) would produce a delay of 13 mm, whereas temperature variations of 0.5°C would produce less than a 1-mm delay. The observations show how streets of water vapor can be identified even when cloud streets are not visible. In fact, no clouds were observed from the weather stations in the interferogram area. Knowledge of these systematic patterns of water vapor can aid in forecasting weather behavior.

Radar interferometry can provide worldwide coverage of mesoscale atmospheric phenomena over land and ice, and easily monitor more exotic features such as gravity waves accompanying fronts. Readily attainable integrated precipitable water amounts over large areas may make pinpoint weather forecasting a possibility. The delay maps could eventually be used by bench forecasters or serve as an additional constraint in variational data assimilation models. Contemporary satellites, however, have an orbital repeat period that is far from ideal for operational applications (*31*), resulting in the loss of coherent phase information over many areas. Proper use of airborne and spaceborne SAR systems with short repeat periods could lead to much greater accuracy in meteorological understanding and forecasting.

References and Notes

1. D. Rind *et al.*, *Nature* **349**, 7500 (1991).
2. K. Emanuel *et al.*, *Bull. Am. Meteorol. Soc.* **76**, 1194 (1995).
3. N. A. Crook, *Mon. Weather Rev.* **124**, 1767 (1996).
4. C. K. Mueller, J. W. Wilson, N. A. Crook, *Weather Forecasting* **8**, 132 (1993).
5. T. M. Weckwerth, J. W. Wilson, R. M. Wakimoto, N. A. Crook, *Mon. Weather Rev.* **124**, 769 (1996).
6. H. A. Zebker, C. L. Werner, P. A. Rosen, S. Hensley, *IEEE Trans. Geosci. Remote Sensing* **32**, 823 (1994).
7. Interferometric phase differences are derived by differencing radar backscatter measurements at the wavelength level, so that if the surface changes on the order of centimeters between observations, the measurement is corrupted (*32*). Because water surfaces are completely different at the centimeter scale for time differences of hours or days, as set by orbital repeat cycles, no meaningful data can be acquired over the ocean.
8. H. A. Zebker and R. M. Goldstein, *J. Geophys. Res.* **91**, 4993 (1986).
9. A. K. Gabriel and R. M. Goldstein, *Int. J. Remote Sensing* **9**, 857 (1988).
10. A. K. Gabriel, R. M. Goldstein, H. A. Zebker, *J. Geophys. Res.* **94**, 9183 (1989).
11. D. Massonnet *et al.*, *Nature* **364**, 138 (1993).
12. D. Massonnet, P. Briole, A. Arnaud, *ibid.* **375**, 567 (1995).
13. R. Goldstein, *Geophys. Res. Lett.* **22**, 2517 (1995).
14. D. Massonnet and K. L. Feigl, *ibid.*, p. 1537.
15. H. Tarayre and D. Massonnet, *ibid.* **23**, 989 (1996).
16. H. A. Zebker, P. A. Rosen, S. Hensley, *J. Geophys. Res.* **102**, 7547 (1997).
17. J. Saastamoinen, *Bull. Geodesique* **106**, 383 (1972).
18. J. L. Davis, T. A. Herring, I. I. Shapiro, A. E. E. Rogers, G. Elgered, *Radio Sci.* **20**, 1593 (1985).
19. G. Elgered, *IEEE Trans. Antennas Propag.* **AP-30**, 502 (1982).
20. Because the SAR phase can only be measured modulo 2π and the satellite position is not known to wavelength accuracy, only lateral gradients in signal delay can be observed. In addition, long wavelength delay gradients, caused by either orbit inaccuracies or hydrostatic or ionospheric gradients, are removed in the process of adjusting the interferogram to a local reference ellipsoid.
21. R. Hanssen, "Atmospheric heterogeneities in ERS tandem SAR interferometry," *Delft Institute for Earth-Oriented Space Research (DEOS) Rep. No. 98.1* (Delft Univ. Press, Delft, 1998).
22. D. Just and R. Bamler, *Appl. Opt.* **33**, 4361 (1994).
23. M. Bevis *et al.*, *J. Geophys. Res.* **97**, 15787 (1992).
24. D. B. Parsons, *J. Atmos. Sci.* **49**, 1810 (1992).
25. J. E. Simpson, *Sea Breeze and Local Wind* (Cambridge Univ. Press, Cambridge, 1994).
26. E. R. Kursinski, G. A. Haij, J. T. Schofield, R. P. Linfield, *J. Geophys. Res.* **102**, 23429 (1997).
27. M. A. LeMone, *J. Atmos. Sci.* **30**, 1077 (1973).
28. R. A. Brown, *Rev. Geophys. Space Phys.* **18**, 683 (1980).
29. M. A. LeMone and W. T. Pennell, *Mon. Weather Rev.* **104**, 524 (1976).
30. J. P. Kuettner, *Tellus* **23**, 404 (1971).
31. Ideally, SAR data should be acquired with multiple short temporal spacings in order to maintain high coherence and permit a large number of interferogram pairs to be generated. Multiple observations give not only better precision in time, but keep coherence and hence data quality high.
32. H. A. Zebker and J. Villasenor, *IEEE Trans. Geosci. Remote Sensing* **30**, 950 (1992).

33. We thank J. Wilson, J. Keeler, F. Fabry, V. Wulfmeyer, and two anonymous reviewers for their helpful comments and suggestions. The ERS SAR data were kindly provided by the European Space Agency and the meteorological data by the Royal Netherlands Meteorological Institute. The German Aerospace Research Establishment is acknowledged for assisting in the data processing.

4 November 1998; accepted 22 January 1999

Tropospheric Aerosol Climate Forcing in Clear-Sky Satellite Observations over the Oceans

J. M. Haywood,[1] V. Ramaswamy,[2]* B. J. Soden[2]

Tropospheric aerosols affect the radiative forcing of Earth's climate, but their variable concentrations complicate an understanding of their global influence. Model-based estimates of aerosol distributions helped reveal spatial patterns indicative of the presence of tropospheric aerosols in the satellite-observed clear-sky solar radiation budget over the world's oceans. The results show that, although geographical signatures due to both natural and anthropogenic aerosols are manifest in the satellite observations, the naturally occurring sea-salt is the leading aerosol contributor to the global-mean clear-sky radiation balance over oceans.

Tropospheric aerosols (*1*, *2*), which include sulfate (*3*, *4*), black carbon (*5*, *6*), organic carbon (*6*), mineral dust (*7*), and sea-salt (*8*, *9*), affect Earth's radiation budget in a significant manner. Predictions of their net radiative effect have proven difficult because aerosol distributions vary greatly in type, space, and time. By reflecting sunlight, the present-day background tropospheric aerosols reduce the solar radiation absorbed by the planet (*10*). Likewise, an increase in anthropogenic aerosols leads to additional reflection, and this has in turn led to a negative radiative forcing of climate change over the past century (*1*). A central issue underlying potential aerosol-climate linkages is verification of the presence of aerosols and their associated radiative effects, both in the context of the present-day climate and climate change scenarios.

[1]Meteorological Research Flight, United Kingdom Meteorological Office, Farnborough, Hants GU14 0LX, UK. [2]Geophysical Fluid Dynamics Laboratory, Princeton University, Princeton, NJ 08542, USA.

*To whom correspondence should be addressed. E-mail: vr@gfdl.gov